

Article

Strength Estimation of Damaged Rock Considering Initial Damage Based on P-Wave Velocity Using Regression Analysis

Xiao Xu ¹, Chuanhua Xu ², Jianhua Hu ^{1,3} , Shaowei Ma ^{1,*} , Yue Li ², Lei Wen ⁴ and Guanping Wen ¹ ¹ School of Resources and Safety Engineering, Central South University, Changsha 410083, China² Sinosteel Maanshan General Institute of Mining Research, Co., Ltd., Maanshan 243000, China³ Zijin School of Geology and Mining, Fuzhou University, Fuzhou 350108, China⁴ School of Architectural Engineering, Chongqing Industry Polytechnic College, Chongqing 401120, China

* Correspondence: mashaowei@csu.edu.cn

Abstract: High dispersion of rock mass strength causes significant difficulties in strength prediction. This study aims to investigate experimentally the strength prediction model for brittle damaged rock with multiscale initial damage based on P-wave velocity using regression analysis. Intact dolomitic limestone was collected from a deep metal mine in Southern China. Rock specimens with different initial damage degrees were prepared through the application of uniaxial compressive stress. Both intact rock and damaged rock specimens were tested for P-wave velocity and uniaxial compressive strength (UCS). The test results indicate that the method of prefabricating initial damage to the rock mass through uniaxial compressive stress is feasible. The UCS values of the damaged rock specimens were correlated with the square of the P-wave velocity (linearly positive) and the initial damage (linearly negative). The parameters of the new strength prediction model have a physical significance, and its results are within the upper and lower limits of the 95% confidence interval of the UCS. The strength prediction model considering multiscale initial damage based on P-wave velocity could reasonably predict the strengths of brittle rock masses.



Citation: Xu, X.; Xu, C.; Hu, J.; Ma, S.; Li, Y.; Wen, L.; Wen, G. Strength Estimation of Damaged Rock Considering Initial Damage Based on P-Wave Velocity Using Regression Analysis. *Sustainability* **2022**, *14*, 14768. <https://doi.org/10.3390/su142214768>

Academic Editor: Chaolin Zhang

Received: 22 October 2022

Accepted: 7 November 2022

Published: 9 November 2022

Publisher's Note: MDPI stays neutral with regard to jurisdictional claims in published maps and institutional affiliations.



Copyright: © 2022 by the authors. Licensee MDPI, Basel, Switzerland. This article is an open access article distributed under the terms and conditions of the Creative Commons Attribution (CC BY) license (<https://creativecommons.org/licenses/by/4.0/>).

Keywords: strength prediction; P-wave velocity; damaged rock; initial damage; uniaxial compression test

1. Introduction

Different degrees of initial fissures render discrete strength distributions in engineering rock masses. The conventional method for obtaining the strength of a rock mass is to average the test results. However, the accuracy of the results depends on the sample size [1,2]. For convenient engineering geology application, the methods for strength prediction of rock masses, e.g., the constitutive model method [3–5], the nonlinear regression method [6], and the multi-factor neural network prediction [7–10], have gained significant attention. Previous studies have investigated the empirical formula method based on P-wave velocity and rock strength [11–14]. Although the empirical formula method has a simple operation procedure and low computational time when using intact rocks during laboratory tests, it is unclear if the applicability of the method can be extrapolated to engineering rock masses.

Typically, a rock is a nonlinear and heterogeneous material. Rock failure is a process involving the occurrence and development of microcracks and formation of connected macro fissures and failure surfaces. In this process, a rock where only microscopic damage has occurred is considered an intact rock [15,16]. The initial damage to a fissured rock mass, without a fractured surface, is assumed macroscopically continuous. Rock masses with various fissure developments can be regarded as damaged rocks with multiscale initial damage [17–20]. According to damage mechanics and elastic wave theory [21–23], it is feasible to characterize the damage to a rock mass through P-wave velocity. Therefore, identifying the impact of multiscale initial damage on the strength of a rock, based on the P-wave velocity, is the key to strength estimation of rock masses.

The conventional method for setting the initial damage to rocks is to prefabricate the fractures. It is difficult to collect natural rock specimens with comparable and controllable initial damages. However, prefabricated fissures with parallel open crack surfaces are significantly different from real cracks and fissures in rock masses [24,25]. Considering the process and occurrence conditions of rock failure in deep rock masses, the multiscale crack propagation state of a rock during vertical compressive loading is consistent with the real initial crack development in the rock masses.

This study aims to experimentally investigate the strength prediction model for brittle damaged rock with multiscale initial damage based on P-wave velocity. Five groups of dolomitic limestone rock specimens, which were collected from a deep metal mine in southern China, were pre-damaged under different uniaxial compressive stresses. Both intact and damaged rock specimens were tested for P-wave velocity. The damaged rock specimens were prepared for uniaxial compressive strength (UCS) tests. A strength prediction model for rock masses, with P-wave velocity and strength, was established and verified with the results from previous studies.

2. Materials and Methods

2.1. Test Instruments and Intact Rock Specimens

UCS tests with a loading control mode were performed in an INSTRON-1346 universal material testing machine, and the P-wave velocity tests were conducted on the ADLINK acoustic wave sensor apparatus, as shown in Figure 1. The instruments were calibrated according to the verification and calibration standard, and the tests were carried out after calibration was qualified.

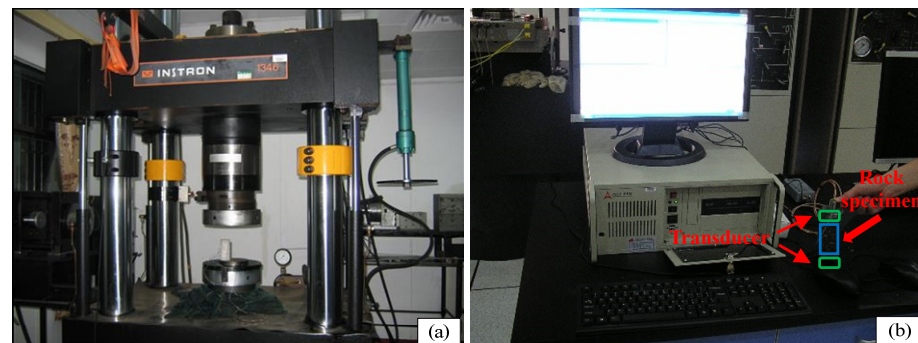


Figure 1. Testing instruments: (a) INSTRON-1346 universal material testing machine; (b) ADLINK acoustic wave sensor apparatus.

Intact rock specimens (dolomitic limestone) were collected from a deep metal mine in Southern China. The specimens were cylindrical with dimensions of $\phi 50 \times 100$ mm, as shown in Figure 2. The density (ρ) was 2704 kg/m^3 , the P-wave velocity (v_p) was 5737 m/s , the elastic modulus (E) was 33.701 GPa , the Poisson's ratio (μ) was 0.253 , and the UCS was 88.139 MPa .

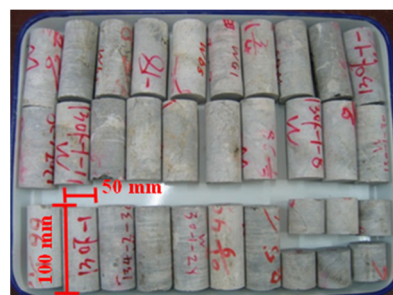


Figure 2. Intact rock specimens.

2.2. Test Procedure

Considering the multiscale crack propagation states of the intact rock during uniaxial compressive loading [26], different uniaxial compressive stresses ($0.25\sigma_0$, $0.40\sigma_0$, $0.50\sigma_0$, $0.65\sigma_0$, and $0.75\sigma_0$) were applied for initial damage to the damaged rock specimens, as shown in Figure 3.

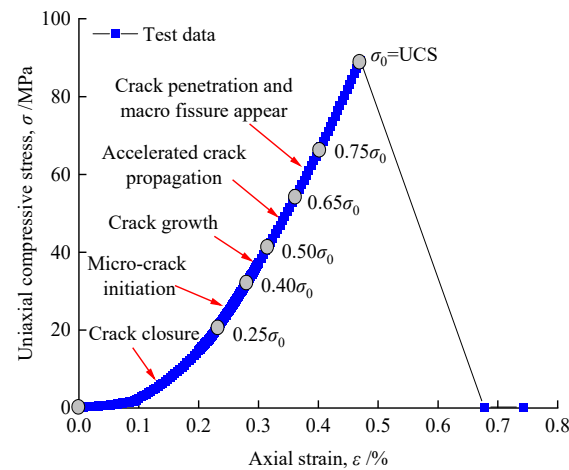


Figure 3. Multiscale crack propagation states of the intact rock during the uniaxial compressive loading. Note that σ is the uniaxial compressive stress (MPa), σ_0 is the uniaxial compressive peak strength of the intact rock ($\sigma_0 = UCS$), and ε is the axial strain (%).

The brittle failure threshold of the rock is $0.75\sigma_0$. When the uniaxial compressive stress exceeds $0.75\sigma_0$, the rock specimen will quickly reach the uniaxial compressive peak strength and lose its bearing capacity [26].

When the uniaxial compressive stress exceeds $0.75\sigma_0$ (the brittle failure threshold of the rock), the rock specimen quickly reaches the uniaxial compressive peak strength and loses its bearing capacity [26].

For each group of damaged rock specimens with different multiscale initial damage degrees ($0.25\sigma_0$, $0.40\sigma_0$, $0.50\sigma_0$, $0.65\sigma_0$, and $0.75\sigma_0$) and the intact rock, a series of UCS tests were conducted on sixty (ten for each group) specimens. The P-wave velocity tests were performed prior to the UCS tests. The test procedure is illustrated in Figure 4.

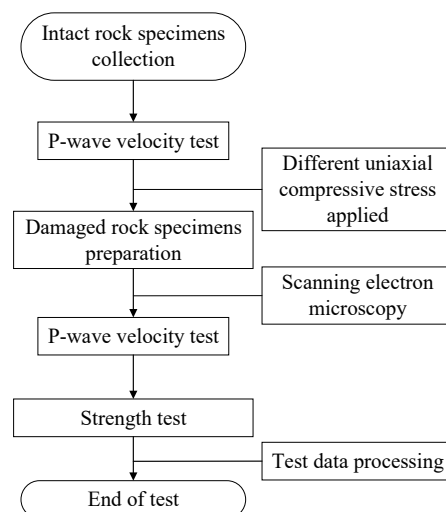


Figure 4. Test procedure.

3. Results

3.1. Analysis of the Typical Stress–Strain Curves

Figure 5 shows the typical stress–strain curves of the intact and damaged rock specimens.

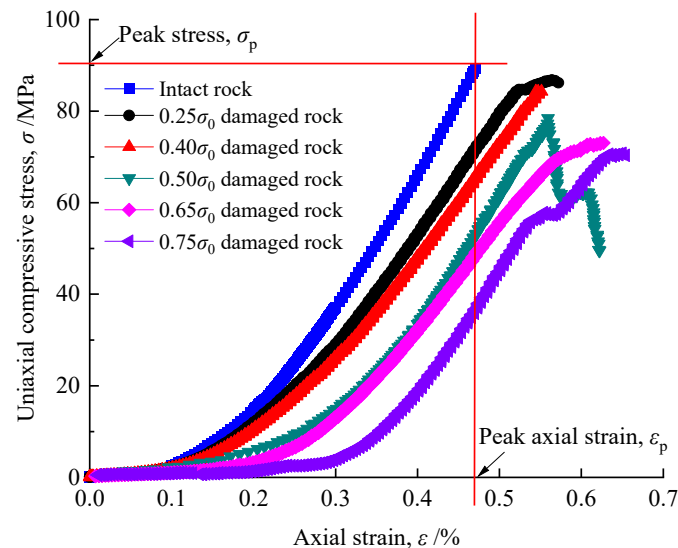


Figure 5. Typical stress–strain curves of the rock specimens.

Figure 5 indicates that all the damaged rock specimens sustained brittle failure, which is consistent with the failure mode of the intact rock. No post-peak strengths were detected. As the degree of the initial damage increased, the peak stress (σ_p) decreased monotonically, and the peak axial strain (ϵ_p) increased significantly. These results are consistent with the results demonstrated by [27].

3.2. Multiscale Initial Damage Investigation

The damaged rock specimens with different initial damage degrees are shown in Figure 6.

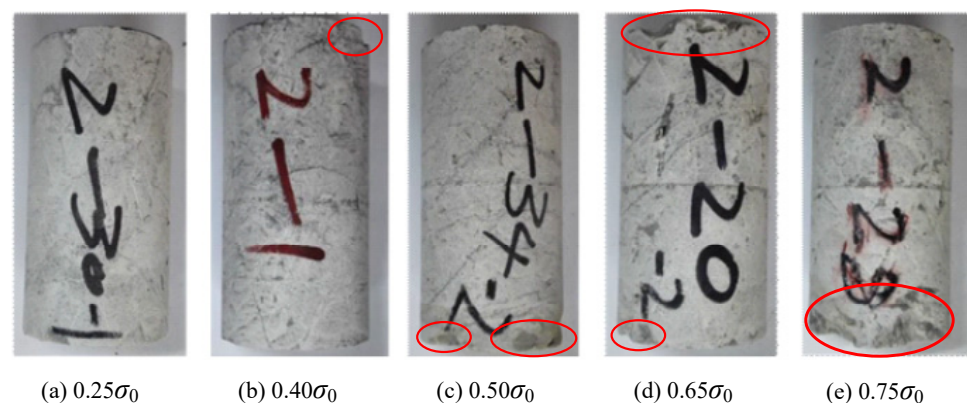


Figure 6. Damaged rock specimens with different initial damage degrees: (a) $0.25\sigma_0$; (b) $0.40\sigma_0$; (c) $0.50\sigma_0$; (d) $0.65\sigma_0$; (e) $0.75\sigma_0$. Note that the red circles represent small areas of macrodamage on the end surfaces of the specimens.

Figure 6 shows that there were distinct macro breakages in the corners of the damaged rock specimens with initial damage degrees of $0.40\sigma_0$, $0.50\sigma_0$, $0.65\sigma_0$, and $0.75\sigma_0$. The greater the initial damage degree, the more small areas of macrodamage on the end surfaces of the damaged rock specimens.

The microcracks inside the damaged rock specimens were observed through scanning electron microscopy (SEM), as shown in Figure 7.

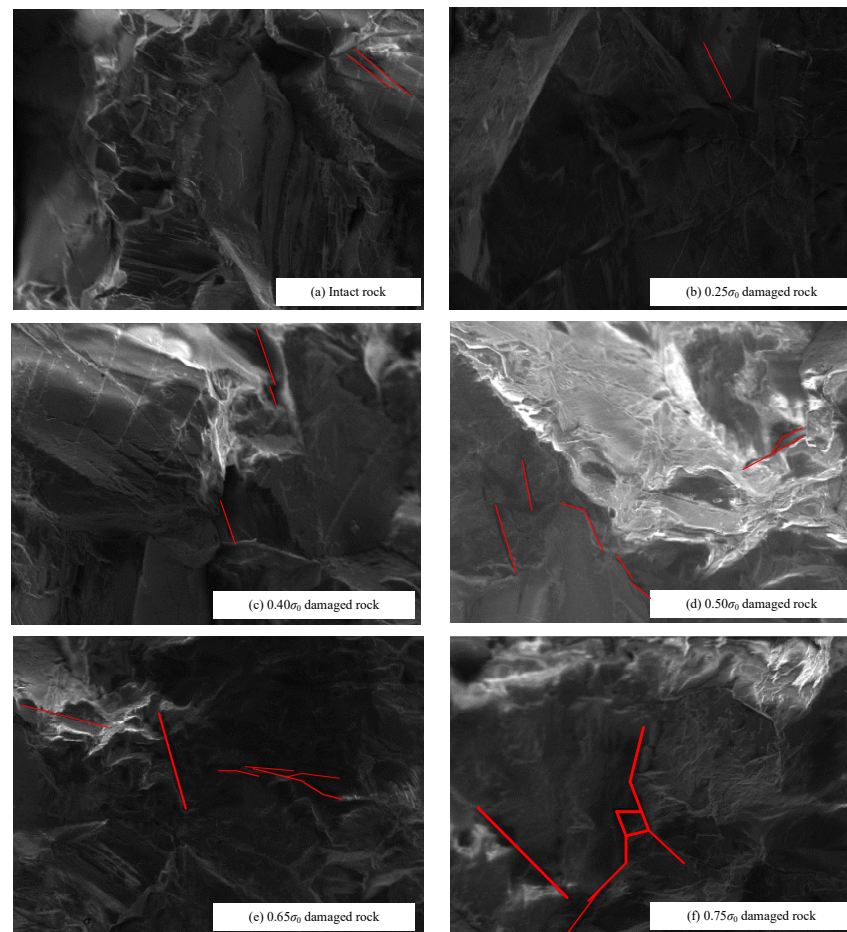


Figure 7. SEM results of the rock specimens (1200 magnification). Note that the red lines with different widths are the cracks identified through SEM.

Figure 7 shows that there were extremely few thin microcracks inside the intact rock and the damaged rock specimens at an initial damage degree of $0.25\sigma_0$. Microcracks started to develop from an initial damage degree of $0.40\sigma_0$, and the initial growth and increase was observed at an initial damage degree of $0.50\sigma_0$. The open crack surfaces at the initial damage degrees of $0.65\sigma_0$ and $0.75\sigma_0$ increased significantly. The multiscale crack morphology is consistent with the findings for a real rock mass reported by [16].

Therefore, it is feasible to prepare the damaged rock specimens with multiscale initial cracks under various uniaxial compressive stresses. The multiscale initial damage to the damaged rock specimens under different uniaxial compressive stresses included microcracks (micron dimension), macro fissures, and small areas of outside breakage (millimeter-scale).

3.3. Multiscale Initial Damage Characterization Based on P-Wave Velocity

According to the elastic wave theory [21], the P-wave velocity in a continuous medium is:

$$v_p = \sqrt{\frac{E(1-\mu)}{\rho(1+\mu)(1-2\mu)}} \quad (1)$$

where v_p is the P-wave velocity (m/s), E is the elastic modulus (GPa), ρ is density (kg/m^3), and μ is the Poisson's ratio.

It was assumed that the multiscale crack propagation process in the rock (as shown in Figure 3) was macroscopically continuous. Therefore, the multiscale initial damage to the rock was macroscopically continuous. Here, multiscale referred to the macroscopic

and microscopic physical dimensions. The principle diagram of the P-wave propagation is shown in Figure 8.

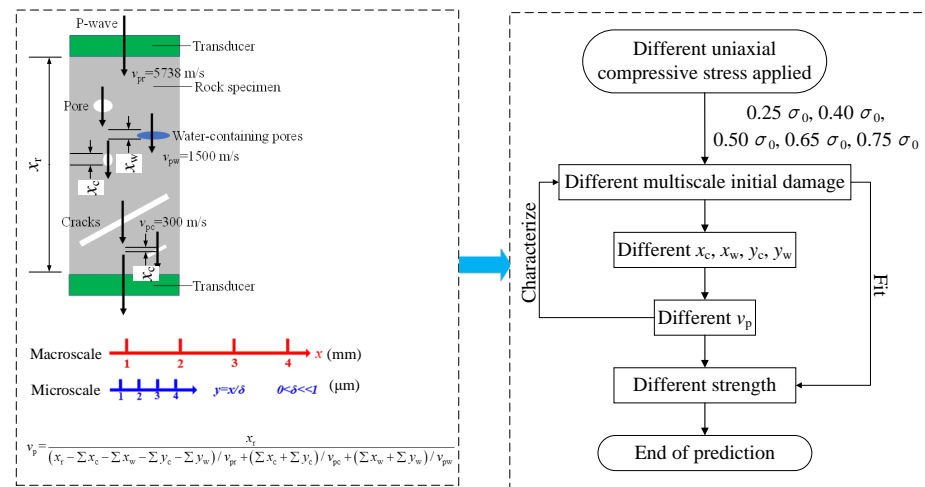


Figure 8. Schematic diagram of P-wave propagation.

Theoretically, the E and μ of a rock change dynamically during loading, as shown in Figure 3 [22]. Therefore, the v_p , E , and μ of the damaged rock specimens with different initial damage degrees were different from each other. It is theoretically feasible to pre-damage an intact rock under a uniaxial compressive stress and then predict the strength of the damaged rock specimens according to the P-wave velocity. The expected values of v_p and E of the intact rock and damaged rock specimens are listed in Table 1.

Table 1. Expected values of v_p and E of the intact rock and damaged rock specimens.

	P-Wave Velocity, $v_p/m \cdot s^{-1}$	Elastic Modulus, E/GPa
Intact rock	5737.45	30.3390
$0.25\sigma_0$ damaged rock	5730.97	30.0992
$0.40\sigma_0$ damaged rock	5638.75	28.7756
$0.50\sigma_0$ damaged rock	5458.41	26.6792
$0.65\sigma_0$ damaged rock	5270.98	23.4593
$0.75\sigma_0$ damaged rock	5166.67	22.5601

Table 1 shows that the v_p and E of the damaged rock specimens with an initial damage degree of $0.25\sigma_0$ approached the results of the intact rock. This is because an initial damage degree of $0.25\sigma_0$ corresponded to the crack closure stage in an intact rock (Figure 3); the damage has not yet occurred, and the E and μ of the rock have not changed substantially.

Rock damage was characterized with the P-wave velocity as follows [28]:

$$D_0 = 1 - \frac{E}{E_0} = 1 - \frac{v_p^2}{v_0^2} = 1 - (1 - \eta)^2 \tag{2}$$

where D_0 is the initial damage in the rock, E is the elastic modulus of the damaged rock specimen, E_0 is the elastic modulus of the intact rock, v_p is the P-wave velocity of the damaged rock specimen, v_0 is the P-wave velocity of the intact rock, $v_p \leq v_0$, and η is the v_p decay rate (%), $0 \leq \eta \leq 1$.

Figure 9 shows the initial damage to the damaged rock specimens.

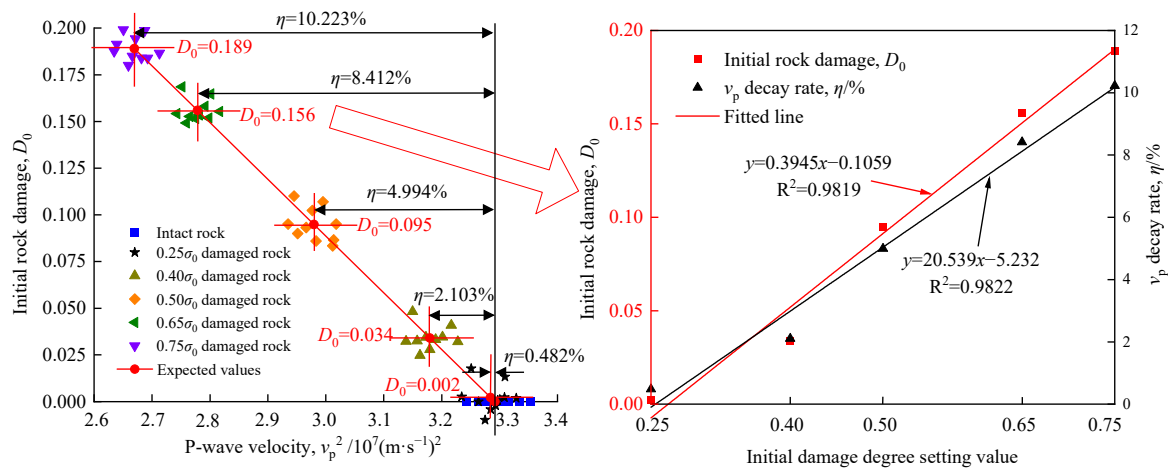


Figure 9. Initial damage to the damaged rock specimens. Note that R^2 is the goodness of fit.

As shown in Figure 9, the actual initial damage to the damaged rock specimens was significantly less than the set initial damage degree values. Nonetheless, as the set initial damage degree value increased, the initial rock damage D_0 linearly increased, as did v_p and the decay rate η . Therefore, it is reasonable to characterize the rock damage by η .

3.4. UCS and the 95% Confidence Interval

It was assumed that the UCS test values of the rock specimens conformed to a normal distribution. The sample size for each rock specimen group was 10. When the confidence level $(1 - \alpha)$ was 95%, the result of the Student's t test was $t_{\alpha/2}(n - 1) = 2.262$ [29]. The UCS of the rock specimens and the 95% confidence intervals are listed in Table 2. X_i is the test sample of UCS, $i = 1, 2, 3, \dots, 10$, \bar{X} is the mean value of X_i , and s^2 is the quadratic mean deviation of X_i . The confidence interval is $[\bar{X} - \frac{s}{\sqrt{n}}t_{\alpha/2}(n - 1), \bar{X} + \frac{s}{\sqrt{n}}t_{\alpha/2}(n - 1)]$.

Table 2. UCS values of the rock specimens and the 95% confidence interval.

Label of Each Group of Specimens	Intact Rock	0.25σ ₀ Damaged Rock	0.40σ ₀ Damaged Rock	0.50σ ₀ Damaged Rock	0.65σ ₀ Damaged Rock	0.75σ ₀ Damaged Rock
No. 1	86.381	85.923	83.246	77.379	72.583	69.581
No. 2	87.284	86.354	83.579	77.726	72.943	69.670
No. 3	88.065	86.927	84.623	78.534	73.058	70.693
No. 4	88.268	87.026	84.865	79.142	73.267	70.761
No. 5	90.697	87.461	85.137	79.390	73.852	71.310
No. 6	89.165	86.239	83.824	77.768	72.583	70.015
No. 7	85.971	86.532	84.116	77.674	72.807	70.417
No. 8	87.029	86.903	84.261	78.033	72.941	70.176
No. 9	88.775	87.064	84.586	78.131	73.367	70.482
No. 10	90.782	87.348	85.116	78.377	73.619	70.906
$\bar{X} = \sum_{i=1}^n X_i$	88.242	86.778	84.335	78.214	73.102	70.4011
$s^2 = \sum_{i=1}^n (X_i - \bar{X})^2 / (n - 1)$	2.740	0.248	0.417	0.427	0.178	0.301
$[\bar{X} - \frac{s}{\sqrt{n}}t_{\alpha/2}(n - 1), \bar{X} + \frac{s}{\sqrt{n}}t_{\alpha/2}(n - 1)]$	[87.058, 89.426]	[86.421, 87.134]	[83.873, 84.797]	[77.748, 78.682]	[72.780, 73.404]	[70.009, 70.794]

Table 2 shows that \bar{X} of the UCS values of the rock specimens is significantly negatively correlated with the initial damage degree. Thus, it is feasible to predict the UCS of a rock mass based on its initial damage.

4. Strength Prediction Model

4.1. Model Fit and Parameter Analysis

The relationship between the UCS and D_0 of the rock specimens is shown in Figure 10.

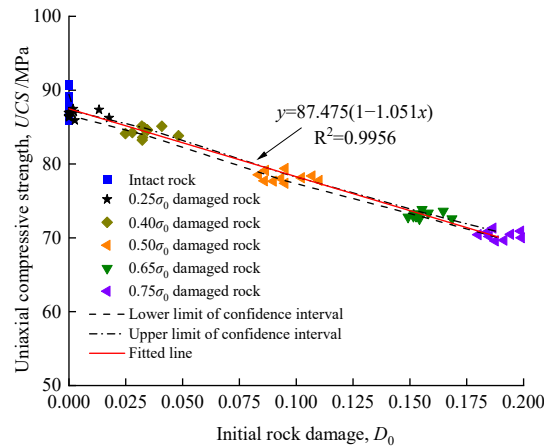


Figure 10. Relationship between UCS and D_0 .

Figure 10 demonstrates that the UCS values of the rock specimens is linearly negatively correlated with D_0 , giving the fitted relationship as:

$$UCS = UCS_0(1 - \delta D_0) \tag{3}$$

where UCS_0 is the theoretical UCS value of the intact rock (MPa), and δ is the correction factor related to the material properties.

Based on Equation (2), the boundary condition of Equation (3) is $0 \leq D_0 \leq 1$.

As shown in Figure 10, the reference values of the strength prediction model parameters of dolomitic limestone were $UCS_0 = 87.475$ MPa and $\delta = 1.051$. The fitted results from Equation (3) were within the upper and lower limits of the 95% confidence interval of the UCS. R^2 was higher than 0.99, which means that Equation (3) is accurate.

Substituting Equation (2) into Equation (3) yields:

$$UCS = UCS_0 \delta \frac{v_p^2}{v_0^2} + UCS_0(1 - \delta) \tag{4}$$

Equation (4) shows the strength prediction model of the rock mass, considering the multiscale initial damage based on the P-wave velocity, as shown in Figure 11.

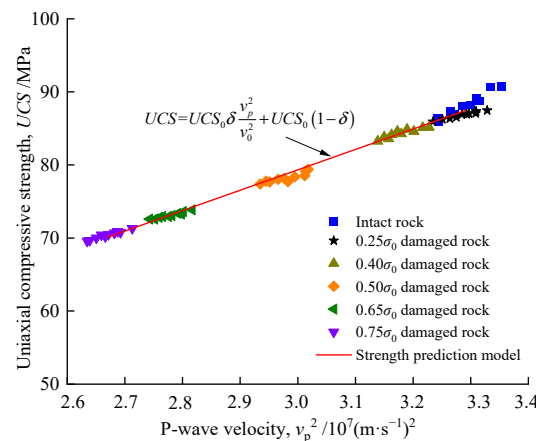


Figure 11. Relationship between UCS and v_p .

The relationship between the UCS and v_p of the rock specimens with different initial damage degrees is shown in Figure 12.

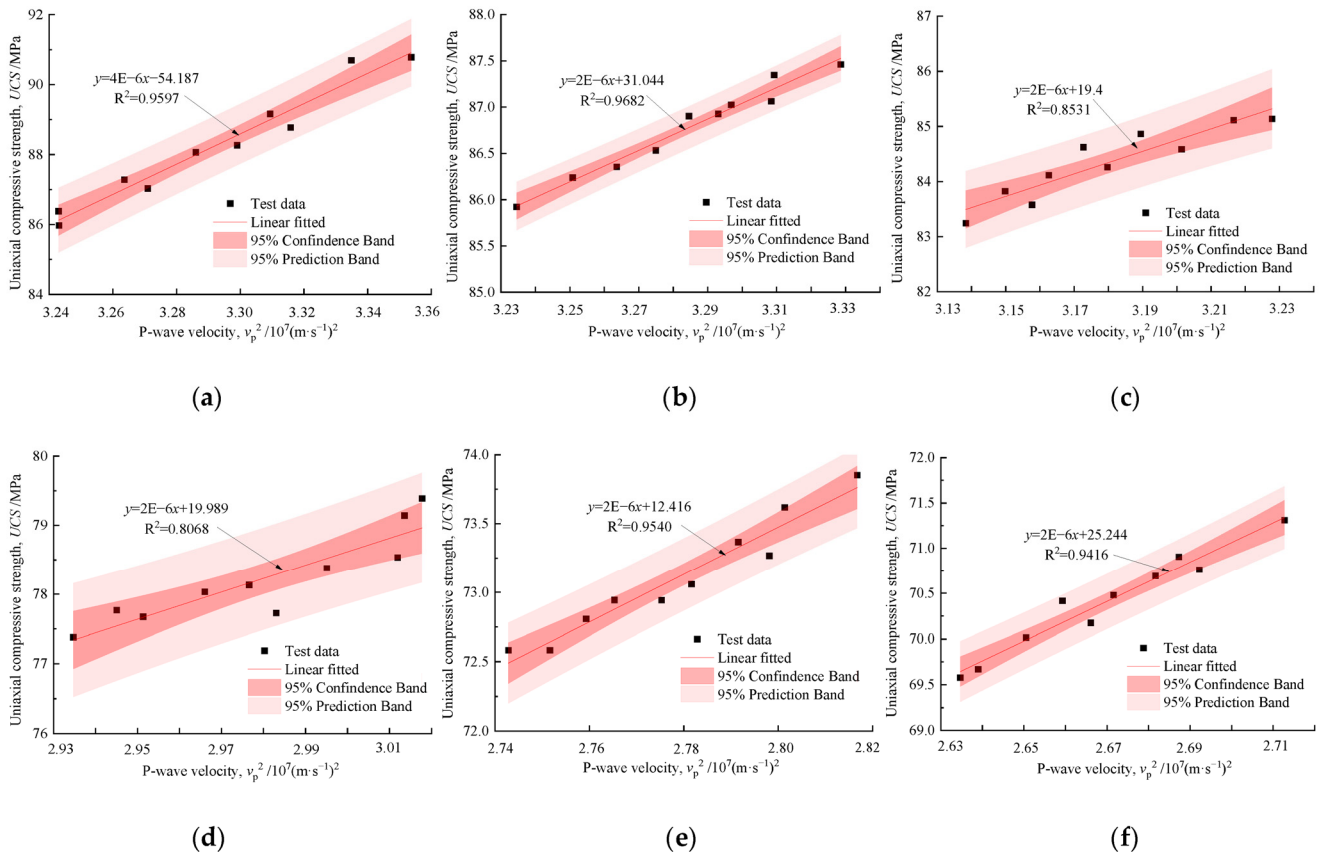


Figure 12. Relationships between UCS and v_p for the rock specimens with different initial damage degrees: (a) 0 (Intact rock); (b) $0.25\sigma_0$; (c) $0.40\sigma_0$; (d) $0.50\sigma_0$; (e) $0.65\sigma_0$; (f) $0.75\sigma_0$.

Figures 11 and 12 show that all the UCS values of the rock masses are linearly positively correlated with the square of v_p .

Figure 12 also indicates the following.

- (1) Without considering the initial damage degree, the fitting curve slopes of the relationships between UCS and v_p are essentially the same, but the intercepts are different. This means that the rock mass needs to be identified and classified in the field applications of engineering geology. The corresponding empirical formula can then be used for strength estimation.
- (2) The parameters of the empirical formulas, as shown in Figure 12, do not have any physical significance. Different empirical formulas can lead to prediction results with slightly different R^2 values. It is particularly subjective and is similar to the direct empirical fitting of the strength and v_p obtained in previous studies [11–14].

Therefore, as shown in Figure 11, the strength prediction model of the rock mass considering multiscale initial damage based on P-wave velocity (Equation (4)) is more reasonable.

4.2. Adaptability Analysis of the Strength Prediction Model

4.2.1. Adaptability of the Prediction Model to Splitting Tensile Strength

Although rock masses are more damaged owing to compression loading in engineering geology projects, the splitting tensile strength (TS) is an important index of rock mass strength considering the impact of mining disturbances [30]. A series of splitting tensile strength tests were carried out in an INSTRON-1346 universal material testing machine (Figure 1) on damaged rock specimens with different initial damage degrees (Figure 6). The

test procedure was the same as that of the UCS tests (Figure 4). The results of the splitting tensile strength tests on the damaged rock specimens with different initial damage degrees are shown in Figure 13.

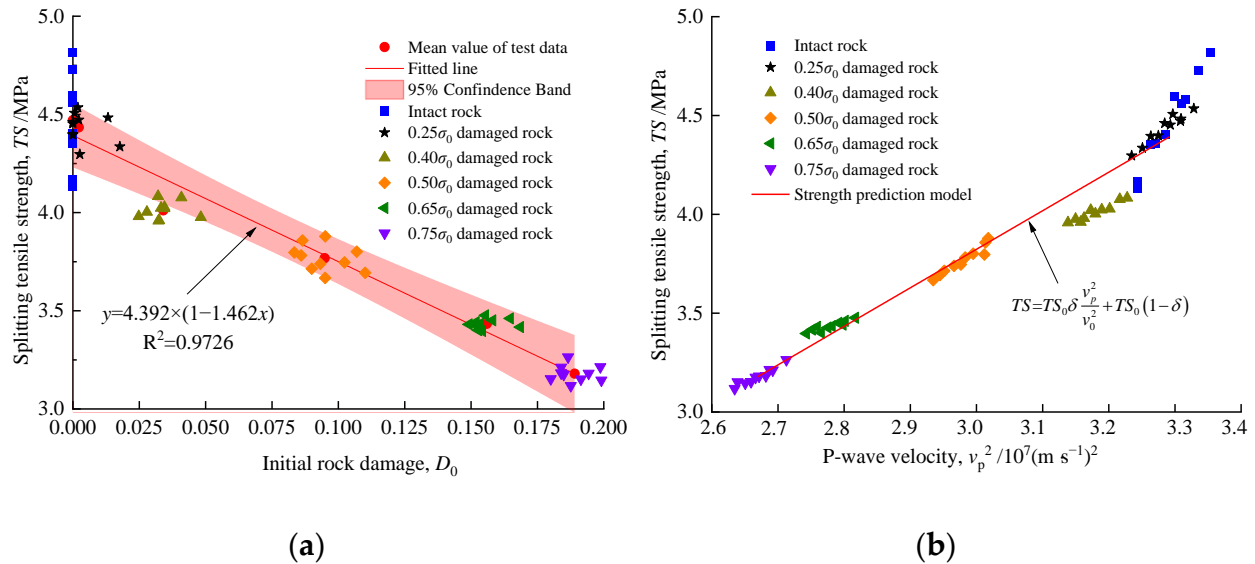


Figure 13. Results of the splitting tensile strength tests: (a) relationship between TS and D_0 ; (b) relationship between TS and v_p .

As shown in Figure 13, the splitting tensile strength prediction model of the rock mass considering multiscale initial damage based on the P-wave velocity can be expressed as

$$TS = TS_0 \delta \frac{v_p^2}{v_0^2} + TS_0 (1 - \delta) \quad (5)$$

where TS_0 is the theoretical TS value of the intact rock (MPa).

The reference values of the splitting tensile strength prediction model parameters for the dolomitic limestone were $TS_0 = 4.392$ MPa and $\delta = 1.462$. Equations (5) and (4) have the same form, and R^2 in Equation (5) was higher than 0.97, indicating a good fit.

The strength prediction model of a rock mass considering multiscale initial damage based on the P-wave velocity can predict both UCS and splitting tensile strength, which can be rewritten as follows:

$$S_R = S_0 \delta \frac{v_p^2}{v_0^2} + S_0 (1 - \delta) \quad (6)$$

where S_R denotes the strength of the rock mass (MPa) and S_0 is the theoretical value of S_R of the intact rock (MPa).

4.2.2. Adaptability of the Prediction Model to Other Rocks

The strength prediction model (Equation (6)) was used to fit the relationships between the S_R and v_p of different rock specimens, as demonstrated in previous studies [22,31–34], as shown in Figures 14–16.

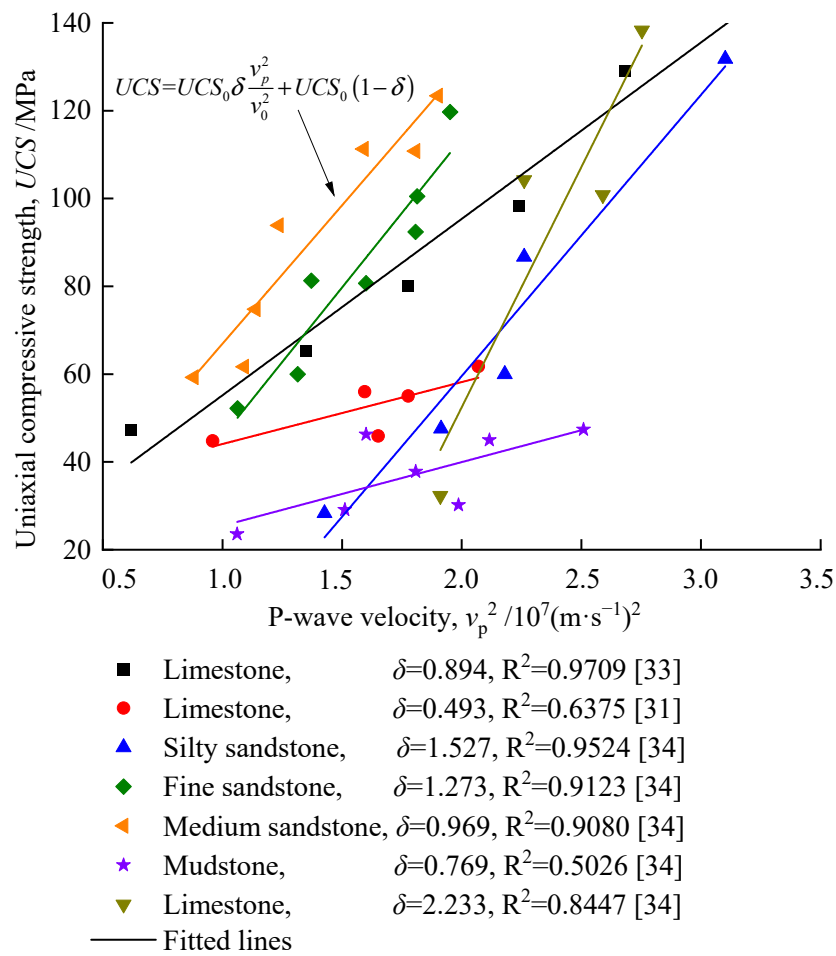


Figure 14. Relationships between UCS and v_p of different rock specimens [31,33,34].

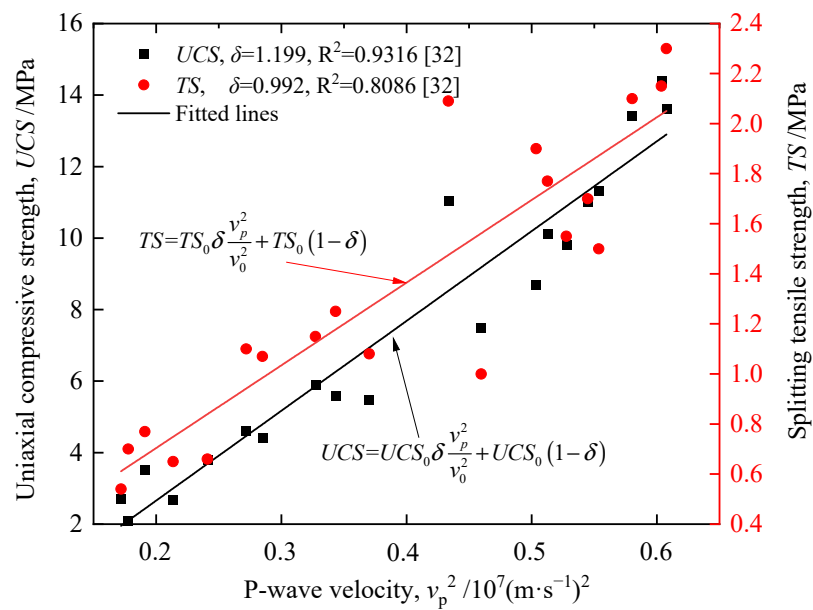


Figure 15. Relationships between UCS, TS, and v_p of the material similar to limestone [32].

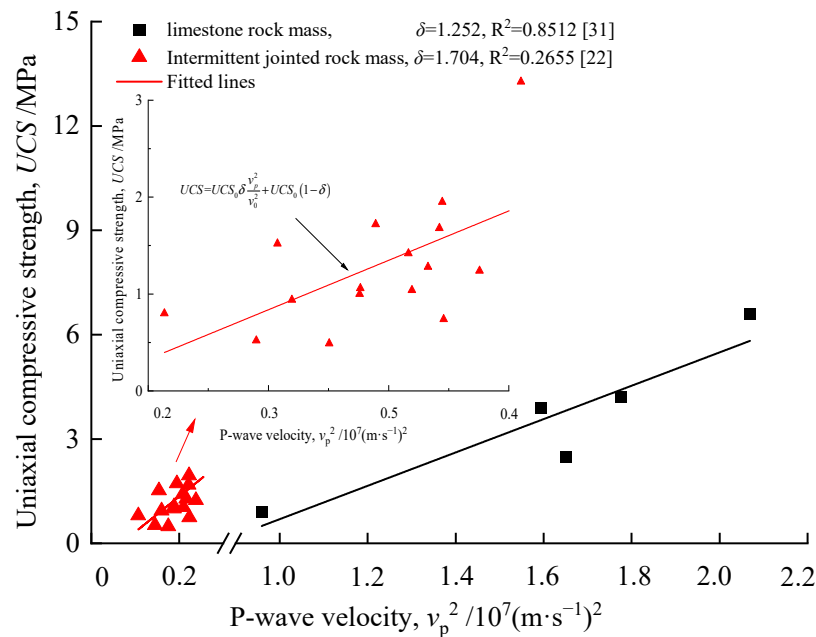


Figure 16. Relationship between UCS and v_p of the rock mass [22,31].

Figures 14–16 indicate the following.

- (1) The fitting lines of the strength prediction model were highly consistent with the test data points of limestone, silty sandstone, fine sandstone, medium sandstone, mudstone, material similar to limestone, and intermittent jointed rock mass. More than 73% of the R^2 values were greater than 0.80, indicating that the strength prediction model could offer good adaptability to other rocks.
- (2) Limited strength data for limestone and limestone rock masses were available in [31] (Figure 14), and the influence of data discreteness cannot be ruled out. The strength failure mode of mudstone in [34] was plastic failure, which differed from that of the brittle rock masses (Figure 15). The R^2 value of the intermittent jointed rock mass reported by [22] was the lowest at 0.2655 (Figure 16). This is because Equation (6) was established on the assumption that the initial damage to the rock mass was macroscopically continuous. However, the initial damage to the intermittent jointed rock mass was macroscopically discontinuous. Therefore, the strength of mudstone and intermittently jointed rock mass cannot be predicted using the strength prediction model for brittle rock masses (Equation (6)).
- (3) Based on the comparability of the test results, only the three groups of rock specimens (silty sandstone, fine sandstone, and medium sandstone) in Figure 14 are compared. The larger the rock particle size, the smaller the correction parameter δ of the model (Equation (6)).

Conclusively, the strength prediction model of the rock mass considering the multiscale initial damage based on the P-wave velocity (Equation (6)) can be used to obtain the strengths of brittle rock masses directly in engineering geology projects.

4.2.3. Comparison with Other Strength Prediction Models

Many previous studies have provided empirical formulas for the relationships between the S_R and v_p of rock masses [11–14]. Comparisons between the theoretical results and test data of the strength prediction model (Equation (6)) and other empirical formula models are shown in Figure 17.

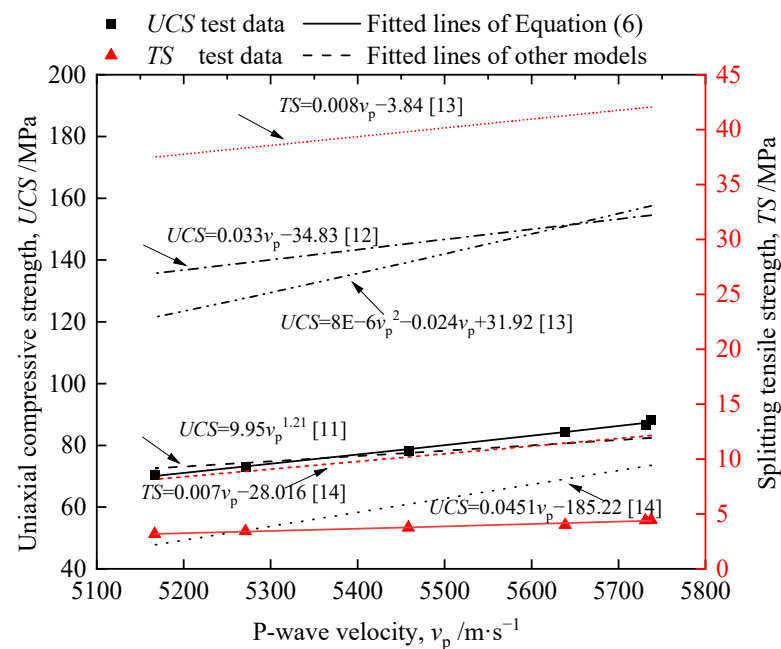


Figure 17. Fitted lines of UCS, TS, and v_p with various empirical formula models [11–14].

Figure 17 shows that only the results by [11] are relatively close to the test data. However, they did not consider the impact of the initial damage degree of the rock mass on the prediction results. In addition, the fitting of the empirical formula requires a large amount of rock strength data. All the coefficients of the empirical formula are fitting parameters, which have no practical significance. The empirical formula used in previous studies cannot be widely used in the strength estimation of other engineering rock masses.

Therefore, the strength prediction model for brittle rock masses considering the multi-scale initial damage based on the P-wave velocity (Equation (6)) is more reasonable and its application is more convenient. There is only one unknown parameter δ in the model (Equation (6)), which is closely related to the material properties of rocks, considering the initial damage characteristics.

5. Discussion

Theoretically, the strength of a rock mass with a fractured surface and joint structure can be obtained using the new strength prediction model established in this study. However, as shown in Figure 16, the R^2 value of the intermittent jointed rock mass reported by [22] was 0.2655, indicating a poor fit. This study limits the assumption that the initial damage to the rock mass is regarded as macroscopically continuous. On the contrary, a rock mass with a fractured surface has a greater variability in strength. A larger sample size is required to obtain predictions that are more accurate. Conclusively, the data distribution of the intermittent jointed rock mass, shown in Figure 16, exhibits a linear growth trend.

Simultaneously, the axial strain generated in the crack-closure stage was higher than that in the intact rock (Figure 5). As the initial damage degree increased, the strain generated in the crack-closure stage increased. This was because there were distinct fractures at the corners of the damaged rock specimens (Figure 6). The interface of the axial actuator of the apparatus (Figure 1) took a long time to fully contact the end faces of the damaged rock specimens. The greater the initial damage degree, the more fractures on the damaged rock specimens, and the larger the strains generated in the crack-closure stage.

In general, the strength prediction model for brittle rock masses established in this study, considering the multiscale initial damage based on the P-wave velocity, is relatively reliable, and its application is more convenient than that of previous models.

6. Conclusions

Based on the results of the uniaxial compressive strength tests and P-wave velocity tests, a new strength prediction model for brittle rock masses, considering multiscale initial damage based on P-wave velocity, was established. The following conclusions can be drawn:

- (1) The strength prediction model for brittle rock masses considering multiscale initial damage based on P-wave velocity was proved to be reasonably practical, and its parameters had physical significance. The larger the rock particle size, the smaller the correction parameter of the strength prediction model.
- (2) The uniaxial compressive strength of the rock mass was linearly positively correlated with the square of the P-wave velocity and linearly inversely correlated with the initial damage. The line-fitted results were within the upper and lower limits of the 95% confidence interval of the UCS.
- (3) As the initial damage degree increased, the initial rock damage increased linearly, the P-wave velocity decay rate increased, the strength decreased monotonically, and the peak axial strain increased significantly. It was proved to be feasible to prepare damaged rock specimens with multiscale initial cracks under various uniaxial compressive stresses.
- (4) The strength prediction model, e.g., the uniaxial compressive strength prediction model and the splitting tensile strength prediction model, could offer good adaptability to other rocks, which can be used to obtain the strength of brittle rock masses directly in engineering geology projects.

Author Contributions: Methodology: X.X., J.H.; Investigation: X.X., S.M., Y.L., G.W.; Writing—Original Draft: X.X., J.H.; Writing—Review and Editing: X.X., C.X., J.H., S.M., Y.L., L.W., G.W.; Project administration: X.X., C.X., J.H., S.M.; Conceptualization: C.X.; Resources: C.X.; Supervision: C.X.; Funding acquisition: C.X.; Formal analysis: J.H.; Validation: S.M., L.W. All authors have read and agreed to the published version of the manuscript.

Funding: This research was funded by National Natural Science Foundation of China with Grant no. 41672298 and the Scientific Research Innovation Project of Postgraduate in Hunan Province of China with Grant no. QL20210068.

Institutional Review Board Statement: Not applicable.

Informed Consent Statement: Not applicable.

Data Availability Statement: Data available on request from the authors. The data that support the findings of this study are available from the corresponding author [Shaowei Ma], upon reasonable request.

Conflicts of Interest: The authors declare no conflict of interest.

References

1. Mishra, D.; Basu, A. Estimation of uniaxial compressive strength of rock materials by index tests using regression analysis and fuzzy inference system. *Eng. Geol.* **2013**, *160*, 54–68. [[CrossRef](#)]
2. Li, W.; Tan, Z.Y. Research on rock strength prediction based on least squares support vector machine. *Geotech. Geol. Eng.* **2017**, *35*, 385–393. [[CrossRef](#)]
3. Yin, P.; Ma, J.; Yan, C.; Huang, L. Estimation of the shear strength of fractured Gosford sandstone based on fractal theory and numerical modelling. *J. Pet. Sci. Eng.* **2019**, *182*, 106278. [[CrossRef](#)]
4. Chen, S.; Cao, X.; Yang, Z. Three Dimensional Statistical Damage Constitutive Model of Rock Based on Griffith Strength Criterion. *Geotech. Geol. Eng.* **2021**, *39*, 5549–5557. [[CrossRef](#)]
5. Shen, J.; Wan, L.; Zuo, J. Non-linear Shear Strength Model for Coal Rocks. *Rock Mech. Rock Eng.* **2019**, *52*, 4123–4132. [[CrossRef](#)]
6. Diamantis, K.; Gartzos, E.; Migiros, G. Study on uniaxial compressive strength, point load strength index, dynamic and physical properties of serpentinites from Central Greece: Test results and empirical relations. *Eng. Geol.* **2009**, *108*, 199–207. [[CrossRef](#)]
7. Tiryaki, B. Predicting intact rock strength for mechanical excavation using multivariate statistics, artificial neural networks, and regression trees. *Eng. Geol.* **2008**, *99*, 51–60. [[CrossRef](#)]

8. Öge, I.F. Prediction of cementitious grout take for a mine shaft permeation by adaptive neuro-fuzzy inference system and multiple regression. *Eng. Geol.* **2017**, *228*, 238–248. [[CrossRef](#)]
9. Xie, C.; Nguyen, H.; Bui, X.-N.; Nguyen, V.-T.; Zhou, J. Predicting roof displacement of roadways in underground coal mines using adaptive neuro-fuzzy inference system optimized by various physics-based optimization algorithms. *J. Rock Mech. Geotech. Eng.* **2021**, *13*, 1452–1465. [[CrossRef](#)]
10. Xie, C.; Nguyen, H.; Choi, Y.; Armaghani, D.J. Optimized functional linked neural network for predicting diaphragm wall deflection induced by braced excavations in clays. *Geosci. Front.* **2022**, *13*, 101313. [[CrossRef](#)]
11. Kahraman, S. Evaluation of simple methods for assessing the uniaxial compressive strength of rock. *Int. J. Rock Mech. Min. Sci.* **2001**, *38*, 981–994. [[CrossRef](#)]
12. Khandelwal, M. Correlating P-wave Velocity with the Physico-Mechanical Properties of Different Rocks. *Pure Appl. Geophys.* **2013**, *170*, 507–514. [[CrossRef](#)]
13. Kurtuluş, C.; Sertçelik, I. Correlating physico-mechanical properties of intact rocks with P-wave velocity. *Acta Geod. Geophys.* **2016**, *51*, 571–582. [[CrossRef](#)]
14. Khajevand, R.; Fereidooni, D. Assessing the empirical correlations between engineering properties and P wave velocity of some sedimentary rock samples from Damghan, northern Iran. *Arab. J. Geosci.* **2018**, *11*, 528. [[CrossRef](#)]
15. Li, X.; Konietzky, H.; Li, X.; Wang, Y. Failure pattern of brittle rock governed by initial microcrack characteristics. *Acta Geotech.* **2019**, *14*, 1437–1457. [[CrossRef](#)]
16. Zhang, Y.; Xu, Y.; Liu, X.; Yao, X.; Wang, S.; Liang, P.; Sun, L.B. Quantitative characterization and mesoscopic study of propagation and evolution of three-dimensional rock fractures based on CT. *Rock. Soil Mech.* **2021**, *42*, 2659–2671. [[CrossRef](#)]
17. Ma, J.; Zhao, G.; Khalili, N. An elastoplastic damage model for fractured porous media. *Mech. Mater.* **2016**, *100*, 41–54. [[CrossRef](#)]
18. Xu, X.; Gao, F.; Zhang, Z. Thermo-mechanical coupling damage constitutive model of rock based on the Hoek–Brown strength criterion. *Int. J. Damage Mech.* **2018**, *27*, 1213–1230. [[CrossRef](#)]
19. Ma, J.; Chen, J.; Chen, W.; Huang, L. A coupled thermal-elastic-plastic-damage model for concrete subjected to dynamic loading. *Int. J. Plast.* **2022**, *153*, 103279. [[CrossRef](#)]
20. Zhang, H.; Guo, P.; Wang, Y.; Zhao, Y.; Lin, H.; Liu, Y.; Shao, Y. Fracture Behavior of Rock with Initial Damage: Theoretical, Experimental, and Numerical Investigations. *Geofluids* **2020**, *2020*, 1–9. [[CrossRef](#)]
21. Tang, X. A unified theory for elastic wave propagation through porous media containing cracks—An extension of Biot’s poroelastic wave theory. *Sci. China Earth Sci.* **2011**, *54*, 1441–1452. [[CrossRef](#)]
22. Zhao, X.C.; Zhao, X.Y.; Guo, J.Q. Experimental study on acoustic and mechanical properties of intermittent jointed rock mass. *Chin. J. Rock. Mech. Eng.* **2020**, *39*, 1409–1419. [[CrossRef](#)]
23. Huang, L.; Liang, J.; Ma, J.; Chen, W. A dynamic bounding surface plasticity damage model for rocks subjected to high strain rates and confinements. *Int. J. Impact Eng.* **2022**, *168*, 104306. [[CrossRef](#)]
24. Fuqi, C.; Zhonghui, L.; Guoai, L.; Yang, W.; Shan, Y.; Shuaijie, L.; Yanhui, K. Influence of prefabricated fissure angle on sandstone damage and infrared radiation temperature characteristics. *J. Geophys. Eng.* **2018**, *15*, 1187–1196. [[CrossRef](#)]
25. Hu, J.; Wen, G.; Lin, Q.; Cao, P.; Li, S. Mechanical properties and crack evolution of double-layer composite rock-like specimens with two parallel fissures under uniaxial compression. *Theor. Appl. Fract. Mech.* **2020**, *108*, 102610. [[CrossRef](#)]
26. Cai, M.; Kaiser, P.K.; Tasaka, Y.; Maejima, T.; Morioka, H.; Minami, M. Generalized crack initiation and crack damage stress thresholds of brittle rock masses near underground excavations. *Int. J. Rock Mech. Min. Sci.* **2004**, *41*, 833–847. [[CrossRef](#)]
27. Hou, R.B.; Zhang, K.; Tao, J. Effects of initial damage on time-dependent behavior of sandstone in uniaxial compressive creep test. *Arch. Min. Sci.* **2019**, *64*, 687–707. [[CrossRef](#)]
28. Yan, C.B.; Li, G.Q.; Chen, D.L. Amended expressions of Hoek-Brown criterion based on blasting cumulative damage effects of rock mass. *Chin. Rock Soil Mech.* **2011**, *32*, 2951–2964. [[CrossRef](#)]
29. Tarasińska, J. Confidence intervals for the power of Student’s *t*-test. *Stat. Probab. Lett.* **2005**, *73*, 125–130. [[CrossRef](#)]
30. Liu, B.; Sang, H.; Wang, Z.; Kang, Y. Experimental Study on the Mechanical Properties of Rock Fracture after Grouting Reinforcement. *Energies* **2020**, *13*, 4814. [[CrossRef](#)]
31. Xia, K.Z.; Chen, C.X.; Liu, X.M.; Zheng, Y.; Zhou, Y.C. Estimation of rock mass mechanical parameters based on ultrasonic velocity of rock mass and hoek-brown criterion and its application to engineering. *Chin. J. Rock. Mech. Eng.* **2013**, *32*, 1458–1466.
32. Liu, T.X.; Long, W.; Hu, L.Y. Application of ultrasonic wave in strength measurement of similar materials of lime-stone. *Chin. J. Transp. Sci. Eng.* **2013**, *29*, 27–31. [[CrossRef](#)]
33. Xie, J. Study on relations between acoustic wave velocity and mechanical parameters for limestone. *Chin. J. Hunan Inst. Sci. Tech. (Nat. Sci.)* **2020**, *33*, 34–37. [[CrossRef](#)]
34. Wang, R.J.L.; Ren, M.; Liu, J.S.; Lipeng, Z.; Shengnan, X.; Ting, S. Study on correlation between rock wave velocity and strength parameters. *Chin. Min. Res. Dev.* **2021**, *41*, 87–91. [[CrossRef](#)]